This is a repository copy of *A simple predictive method for evaluating damping from thin viscoelastic layers in structures*.

White Rose Research Online URL for this paper:
https://eprints.whiterose.ac.uk/221195/

Version: Accepted Version

A simple predictive method for evaluating damping from thin viscoelastic layers in structures

F. Terzioglu [1], J.A. Rongong [1]
[1] The University of Sheffield, Department of Mechanical Engineering,
Engineering Heartspace, Sir Frederick Mappin Building, Mappin Street,
S1 3JD, Sheffield, United Kingdom
e-mail: **f.terzioglu@sheffield.ac.uk, j.a.rongong@sheffield.ac.uk**

Abstract

This work presents a simple approach based on a three-spring model and the modal strain energy method for predicting the dissipative influence of thin viscoelastic layers on the vibration properties of structures. The approach estimates the ratio of strain energy in the viscoelastic component to the overall structure without explicitly modelling the layer. This involves identifying the sensitivity of the structure to stiffness changes of the layer and fitting an equivalent metamodel constructed from series and parallel springs. By making use of the elastic-viscoelastic correspondence principle, the damping of the system for any set of viscoelastic properties can then be obtained easily.

1   Introduction

Thin viscoelastic layers are often present in mechanical components in the form of adhesive joints or are deliberately inserted as damping layers into structures. Their dissipative properties can provide an efficient way to attenuate the dynamic response thereby mitigating destructive resonant vibrations and reducing noise levels. Accurate estimation of the damping levels that such layers contribute is therefore important for structural design and optimisation.

Numerous studies have been carried out to develop predictive methods for assessing the damping influence of viscoelastic layers in structures. The Ross-Kerwin-Ungar (RKU) model is one of the pioneering works which provides an approach to predict the damping levels of a beam enhanced with constrained-layer-damping (CLD) [1,2].While RKU and related models provide high accuracy efficiently, they are limited to simple geometries. Analysis of more complex structures is usually carried out via the Finite Element Method (FEM) with the discretised numerical models being generated directly from computer aided design drawings. One approach has been to develop special multi-layer shell elements that enable large shear deformations in the viscoelastic layer [3]. While these elements have been useful for analysing thin shell-type structures with parallel damping layers, they are not suitable for more complex configurations and are not widely available in commercial software. Whilst three dimensional elements can be used [4], adding such layers explicitly within a numerical model can be expensive and time consuming, particularly for complicated structures having many components connected by viscoelastic layers. This can lead analysts either to neglect the layer and underestimate the damping present, or to develop highly detailed models that are unsuitable for design and optimisation studies.

As an alternative to geometrically representative models, the three-spring estimation [5] was originally introduced as a computationally efficient approach to predict the damping levels of beams treated with CLD. In this approach, the overall stiffness of beam with CLD was represented by a parallel and series three-spring assembly where the stiffnesses of the beam, constraining layer and viscoelastic layer were each represented by a spring. The elastic-viscoelastic correspondence principle was then invoked to obtain estimates of the damping. It should be noted that a modified version of this approach also exists which includes the damping behaviours of layers other than the viscoelastic layer [6]. The advantage of the three-spring approach was that it could represent more complicated cross-sections such as cylinders and tubes [5].

However, in this approach, the stiffness of each spring had to be expressed explicitly and this would vary depending on the deformation pattern considered. As a result, this approach, in its current form, could not be applied easily to more complicated engineering structures.

This study introduces a new approach based on the three-spring model to predict the modal damping ratios of structures with thin viscoelastic layers. Rather than attempting to define an explicit expression of the spring stiffness, this approach depends on the sensitivity of the natural frequencies to the stiffness of the viscoelastic layers. The validity of the approach is first demonstrated on a well-understood structure: a beam with CLD. Results from the new approach are shown to match those generated using the established RKU model. It is then applied to a more complicated component that contains many adhesive joints. This is a rotor from an advanced electrical machine which comprises a cylindrical composite frame into which are bonded a series of laminated pole-pieces that align with the axis of rotation. Modal damping ratios predicted using this approach are compared with those obtained experimentally over a range of temperatures.

2 Three-spring modelling approach

2.1 Theoretical model

A vibration mode of a structure can be modelled as a simple undamped SDOF system which only involves an effective mass, m and an effective spring, k. To incorporate the effect of thin viscoelastic layers (assumed to be inserted into the structure), the effective spring can be decomposed to three springs where two springs with stiffnesses of k_v and k_s are in series forming a link that is parallel to a third spring whose stiffness is k_p as shown in Figure 1.

Simple SDOF representation of a structural mode

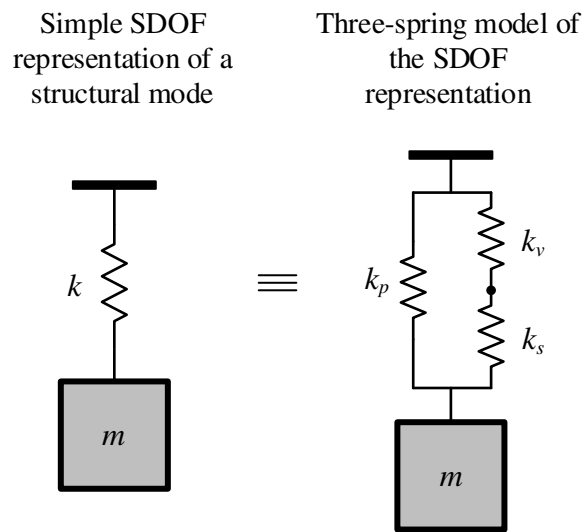Three-spring model of the SDOF representation

Figure 1: Three-spring model of a structural mode.

Using the three-spring model, the effective spring stiffness is determined as:

$$k = k_p + k_v k_s / \left(k_v + k_s \right)$$

(1)

Employing the elastic-viscoelastic correspondence principle, the three-spring model is a very simple way to approximate the effects of the presence of a viscoelastic damping element in a structure. In the original approach [5], where various beams with viscoelastic layers are interested, it is considered that k_p is the primary beam stiffness, k_s is the stiffness of the elastic constraining layer and k_v represents the complex stiffness of the viscoelastic layer. It should be noted here that the original approach was based on the explicit expression of these stiffness terms by utilising the bending behaviour of beams. The approach introduced in this study considers applying the three-spring model for the arbitrary structures with thin viscoelastic layers

where the stiffness terms of the three-spring model cannot be explicitly expressed. Therefore, k_p and k_s cannot be interpreted to the same physical equivalents as in the original approach.

Supposing that the damping of the structure only arises from the viscoelastic layers used, the damping ratio of a structural mode, ζ, is obtained utilising the modal strain energy method [2] as:

$$\zeta = \left(\eta_v / 2\right) U_v / U \tag{2}$$

where η_v is the loss factor of the viscoelastic material, U_v is the modal strain energy of the viscoelastic layers and U is the modal strain energy of the structure with the viscoelastic layers. Note that Equation (2) is only exact if the mode shapes are complex to allow for the presence of damping. However, the common approximation in the Modal Strain Energy method is to assume the modes are real. While this introduces potential errors [7] various methods have been developed to address this.

Employing the three-spring model, the modal strain energies are determined as:

$$U_v = 0.5 k_v x_v^2 \tag{3}$$

$$U = 0.5 k x^2 = 0.5 \left(k_p + k_v k_s / \left(k_v + k_s\right)\right) x^2 \tag{4}$$

where x_v represents the deformation of the spring, k_v, in the three-spring model, and x represents the deformation of the effective spring, k. As the spring force in the series branch of the three-spring model is the same in both springs (k_v and k_s), x_v is written in terms of x as:

$$x_v = x k_s / \left(k_v + k_s\right) \tag{5}$$

Using the relations given in Equations (3)-(5), the modal strain energy ratio, U_v/U is obtained as:

$$U_v / U = 1 / \left(\left(k_p / k_s + 1\right) k_v / k_s + k_p / k_v + 2 k_p / k_s + 1\right) \tag{6}$$

Equation (2) and (6) indicate that the equivalent three-spring model parameters k_p/k_s and k_v/k_s should be known to obtain the damping ratio of a structural mode depending on the damping ratio of the viscoelastic material damping ratio.

2.2   Evaluation of the modal strain energy ratio

The parameters, k_p/k_s and k_v/k_s can be determined by simply investigating the sensitivity of k to k_v. The typical characteristic of k shows a "s" shaped curve as a function of k_v/k_s as illustrated in Figure 2a. It can be seen that k changes from k_p when $k_v \rightarrow 0$ to $(k_p/k_s+1)k_s$ when $k_v \rightarrow \infty$ and becomes equal to $(k_p/k_s+0.5)k_s$ when $k_v = k_s$. These are important observations that can be used to generate a three-spring model fit when the sensitivity of k to k_v is obtained.

Once the three-spring model fit is achieved, U_v/U can either be calculated using Equation (6) or by obtaining the logarithmic gradient of k with respect to k_v as:

$$U_v / U = d \left(\log_e \left(k\right)\right) / d \left(\log_e \left(k_v\right)\right) \tag{7}$$

Figure 2b demonstrates the typical characteristic of U_v/U as a function of k_v/k_s supposing that $k_p/k_s = 3$. As can be seen, Equation (7) produces the same curve as the curve calculated using Equation (6), and they both show an inverted "u" shape.

The parameters, k_p/k_s and k_v/k_s are specific to the structural mode considered. Therefore, if the effective mass of the vibration mode remains constant, the sensitivity of k to k_v is the sensitivity of the square of the mode frequency to k_v. This can allow the determination of k_p/k_s and k_v/k_s (thus the three-spring modal fit) by conducting modal analysis of the system using FEM or even through experimental modal testing if the elasticity level can be varied. This indicates that the three-spring model approach presented here can be implemented for any structure having thin viscoelastic layers to predict the modal strain energy ratio, and thus the modal damping ratio.
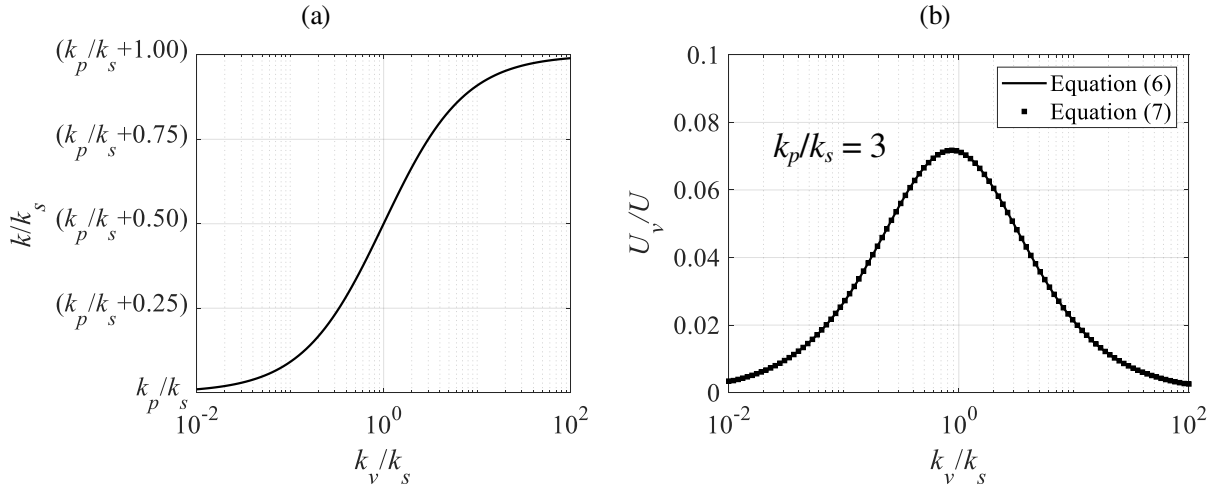
Figure 2: Typical characteristics in three-spring model as a function of viscoelastic component stiffness: (a) effective stiffness and (b) strain energy ratio.

3 Three-spring model for a beam with constrained-layer-damping

To show the accuracy of the three-spring model approach for estimating U_v/U, a study was conducted for the first two modes of a rectangular beam with CLD and free boundaries. This simple beam example was selected as the first case study because its U_v/U could be accurately obtained for each mode by using RKU model [1,2] and thus used for comparison. The geometric and material properties of the structure considered in this study is provided in Table 1.

Table 1: Material and geometric properties of the beam-with-CLD application.

Part	Property	Unit	Value
Beam and constraining layer	Young's modulus	GPa	70
	Density	kg/m^3	2700
	Length	mm	400
	Width	mm	25
	Beam thickness	mm	4
	CL thickness	mm	0.25
Viscoelastic layer	Young's modulus	Pa	various
	Poisson's ratio	-	0.4
	Loss factor	-	0.1
	Density	kg/m^3	1000
	Thickness	mm	0.05

The FEM model of the beam with the CLD was constructed via the commercial software Ansys [8] to obtain the three-spring model fit for each mode. The beam was modelled using standard 20-node solid elements whilst the constraining layer was modelled using standard 8-node shell element offset from the surface of the beam. The size of each element edge was set to 1 mm. The penalty method was used to represent the varying elasticity level of the thin viscoelastic layer inserted between the beam and the constraining layer by changing the contact stiffness. The first two free modes of the beam rigidly connected to the constraining layer (without the viscoelastic layer) obtained by the RKU and FEM models are shown in Table 2.

Table 2: First two free bending modes of the beam with a rigidly bonded constraining layer.

Mode number	Mode shape	Mode frequency - RKU [Hz]	Mode frequency - FEM [Hz]
1		139.3	137.7
2		384	379

To obtain the sensitivity of k to k_v for each mode, the RKU model was run for various levels of viscoelastic material elasticity whilst the FEM model was simulated for various contact stiffness. The reduction in the mode frequencies with respect to those presented in Table 2 is shown in Figure 3. In the graphs, the RKU results are given as a function of $k_v = E_v f_{geo}$ where E_v is the varying elastic modulus of the viscoelastic layer and f_{geo} is the constant geometric coefficient which represents the geometric property of the viscoelastic layer. The FEM results are presented as a function of $k_v = f_c k_c$ where f_c is the varying scaling factor that determines the level of Penalty method stiffness and k_c is the constant default contact stiffness of the Penalty method calculated by the software depending on the properties of the contacting elements. Figure 3 demonstrates that both models exhibit the similar characteristics for each mode. The mode frequencies reduce by decreasing k_v but at different rate depending on the level of k_v.
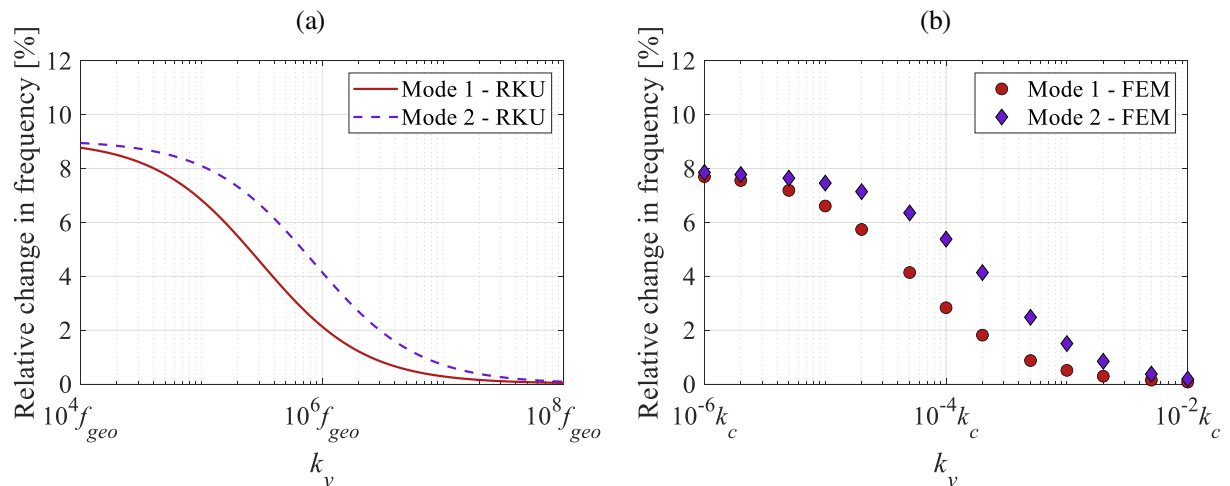

Figure 3: Mode frequency changes of the beam-with-CLD obtained from: (a) RKU model and (b) FEM model.

As the effective mass properties (m_1 and m_2) are maintained for each mode, the sensitivity of k to k_v is calculated as shown in Figure 4. The piece-wise cubic interpolation was applied to the calculated FEM results to obtain the FEM result curves. As can be seen, all curves exhibit the "s" shape characteristic stated in the methodology. It should be noted here that although U_v/U was directly obtained for various E_v in the RKU model the sensitivity of k to k_v was also computed by the RKU model to obtain the three-spring model fit by using the RKU mode frequencies.

In order to fit the three-spring model and simulate the general case given in Figure 2a, the three conditions established for Figure 2a were applied to each case shown in Figure 4. The three-spring model parameters calculated for each case are listed in Table 3. Using these three-spring model parameters, U_v/U was evaluated using both RKU and FEM for each mode as in Figure 5. As can be seen from this figure, the three-spring fitted U_v/U curves computed by using the RKU frequencies match with those obtained directly by the RKU model. This shows the accuracy level of the three-spring model approach presented in this paper. It can also be seen from this figure that the three-spring fitted U_v/U curves obtained by using the FEM

frequencies underestimates the RKU U_v/U curves. This results from the differences in the mode frequencies observed between the FEM and RKU models.
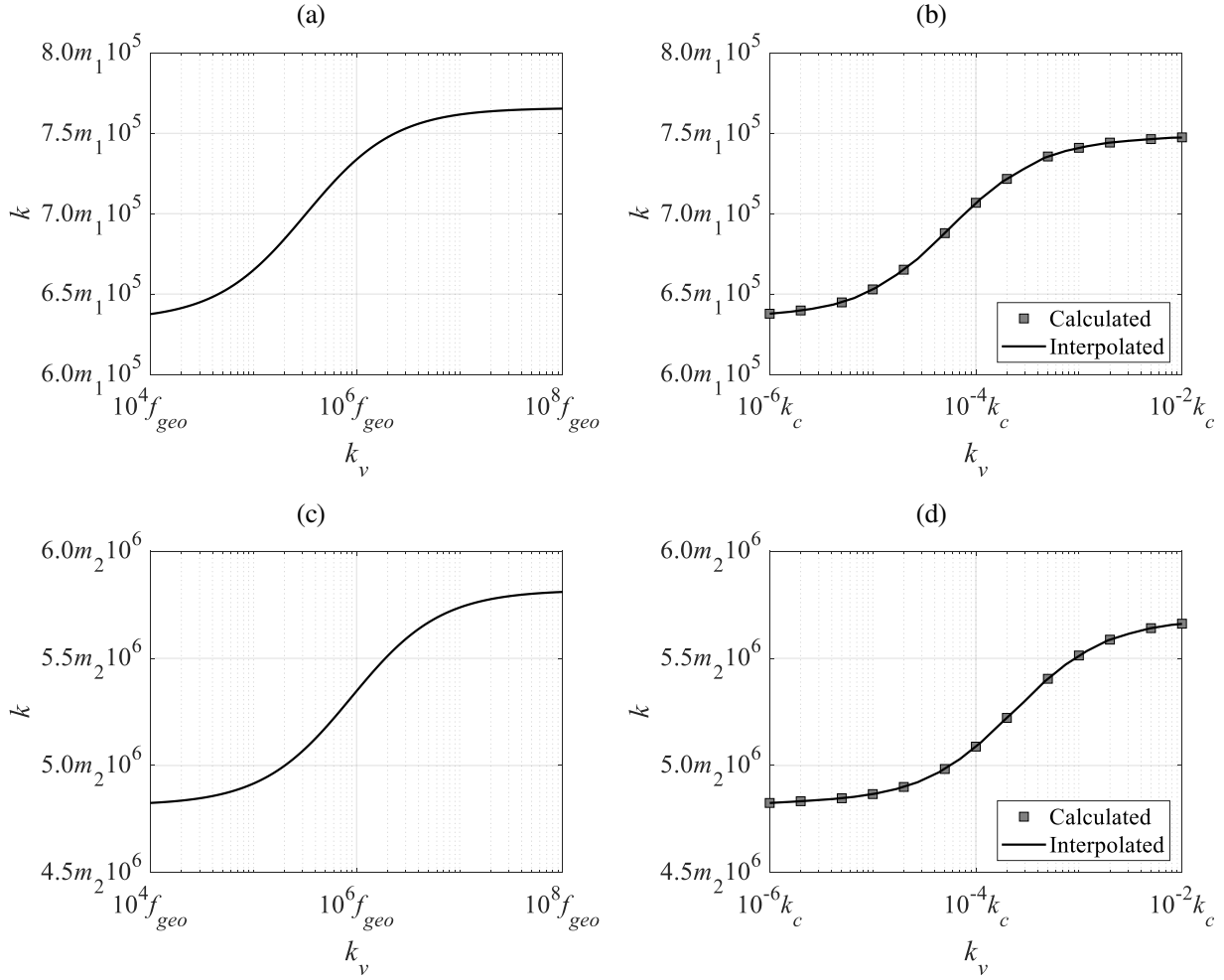

Figure 4: Effective stiffness sensitivity of the beam-with-CLD to the viscoelastic layer stiffness (a) first mode – RKU model, (b) first mode – FEM model, (c) second mode – RKU model and (d) second mode – FEM model.

Table 3: Three-spring model fit parameters of the beam-with-CLD.

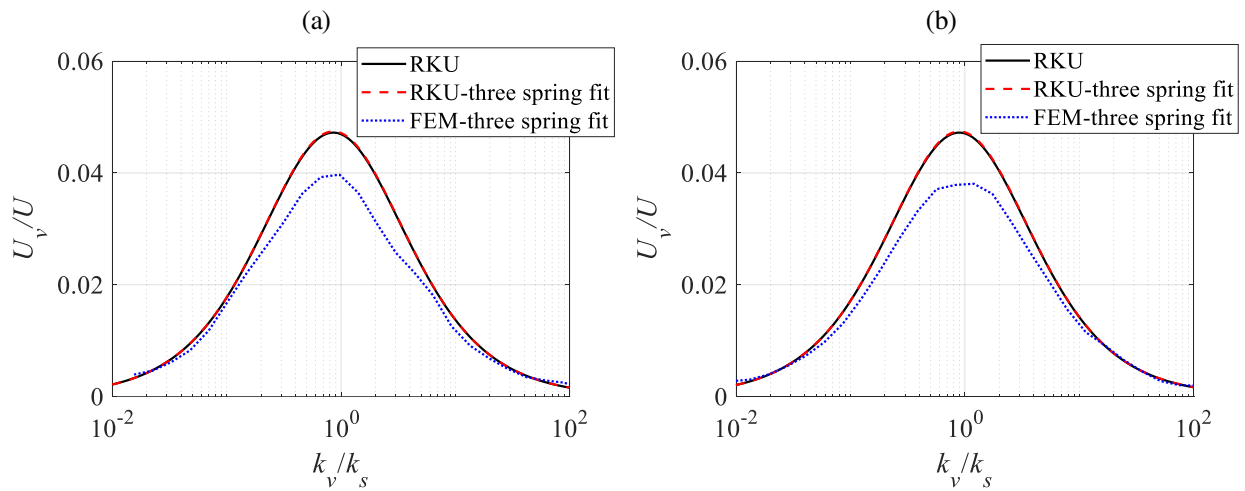| Model	Mode No	Three-spring model fit parameters		
		k_s in terms of effective mass	k_s in terms of varying elastic property	k_p/k_s
RKU	1	$1.28m_1 10^5$	$3.41 f_{geo} 10^5$	4.98
	2	$1.00m_2 10^6$	$9.01 f_{geo} 10^5$	4.82
FEM	1	$1.11m_1 10^5$	$6.44 k_c 10^{-5}$	5.75
	2	$0.85m_2 10^6$	$2.35 k_c 10^{-4}$	5.68

Figure 5: Strain energy ratio comparisons of the beam-with-CLD: (a) first mode and (b) second mode.

4 Damping prediction of a rotor with viscoelastic adhesive joints

To demonstrate the three-spring model fit implemented for the structural modes of a more complicated machine component and compare the damping predictions with experimental results, a pole-piece rotor (PPR) was considered as a second case study. As shown in Figure 6, the rotor was formed by a cylindrical composite casing, 60 laminated pole-pieces that were bonded into the casing slots by using a viscoelastic epoxy adhesive and a composite end plate.

4.1 Three-spring model fit of the rotor

In order to generate the three-spring model fit, a FEM model of the PPR was constructed as can also be seen in Figure 6. The FEM model was composed of the standard 20-node solid and 10-node tetrahedral element types. Rather than model the adhesive layers, the penalty method was employed to represent the varying elasticity level of the thin adhesive layers inserted between the pole-pieces and the casing slots by changing the contact stiffness.
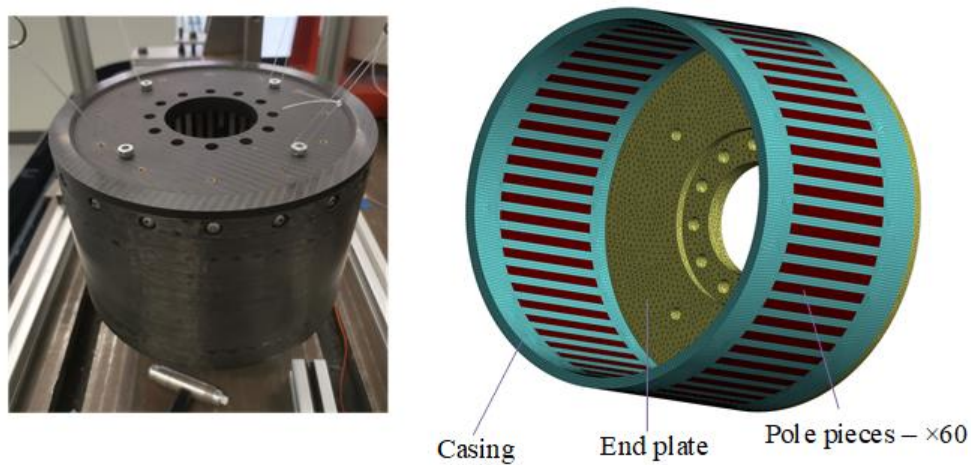

Figure 6: Picture of the PPR and its FEM model.

As the adhesive layers were used in the casing slots, the first two free casing-dominated modes were considered for the three-spring model fitting process. The eigen-solution of the FEM model was executed for varying contact stiffness between the pole-pieces and the casing to compute the reduction levels in the mode frequencies with respect to the rigid connection case. The mode shapes and the corresponding mode frequency changes can be found in Figure 7. As can be seen from the results, both mode frequencies decrease as k_v reduces with different rate depending on the level of k_v. The second mode is more sensitive to the change in k_v than the firs mode as its mode shape involves more relative motion on the adhesive regions.
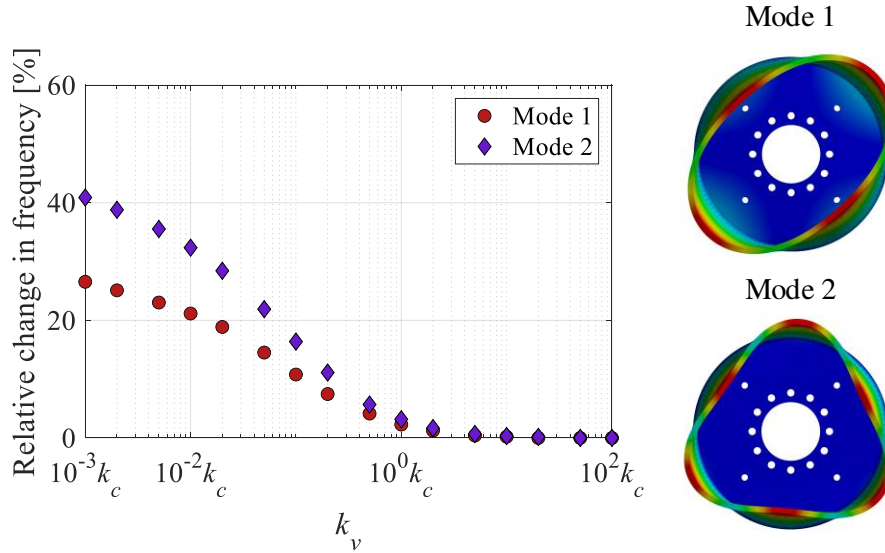

Figure 7: Mode frequency changes of the PPR.

Supposing that the effective mass properties (m_1 and m_2) are maintained for each mode, the sensitivity of k to k_v is obtained as demonstrated in Figure 8. Note that the piece-wise cubic interpolation was used to obtain the resulting curves. Similar to the observation in the beam with a CLD case study, both curves show the "s" shape characteristic.
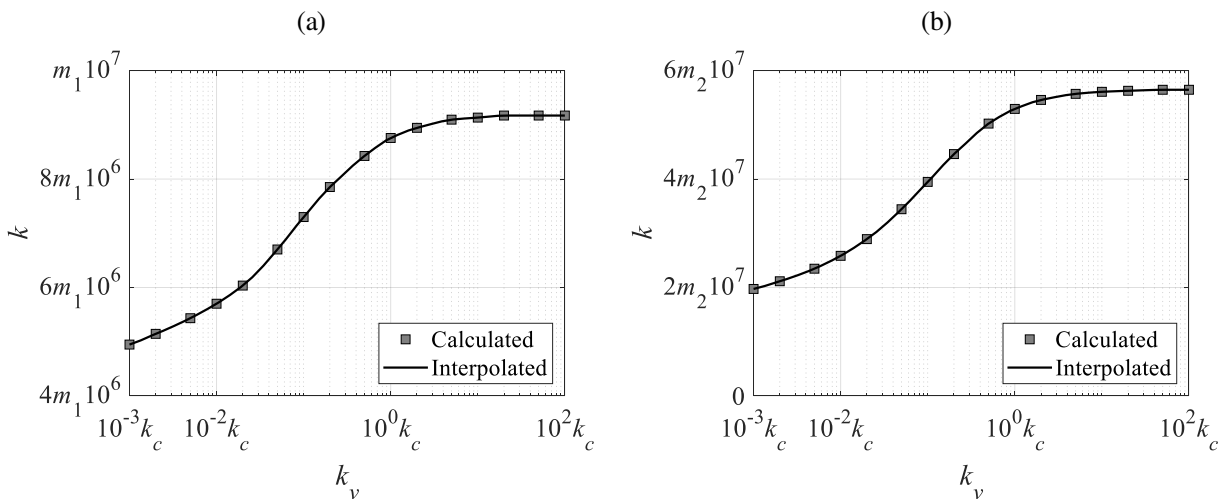

Figure 8: Effective stiffness sensitivity of the PPR to the adhesive stiffness (a) first mode and (b) second mode.

The three-spring model fit parameters were computed for each mode as provided in Table 1. Utilising these three-spring model fit parameters, the U_v/U curves were obtained for both modes as shown in Figure 9. This

plot shows that the second mode of the PPR produces larger U_v/U at any level of the adhesive elasticity. This means that the second mode has the potential to exhibit larger damping property than the first mode. However, Equation (2) indicates that the exact level of modal damping also depends on the damping of the viscoelastic material (i.e., adhesive in this case).

Table 4: Three-spring model fit parameters of the PPR.

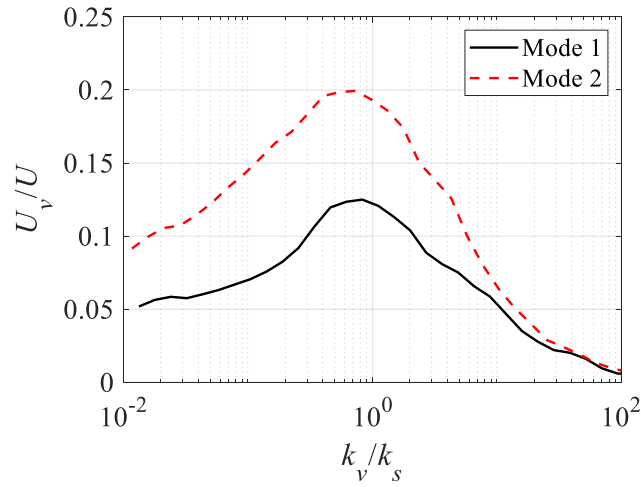| Mode No	Three-spring model fit parameters		
	k_s in terms of effective mass	k_s in terms of varying elastic property	k_p/k_s
1	$4.22m_1 10^6$	$7.49k_c 10^{-2}$	1.17
2	$3.68m_2 10^7$	$8.52k_c 10^{-2}$	0.54

Figure 9: Strain energy ratios of the PPR.

4.2 Material characterisation of viscoelastic adhesive

To predict the modal damping ratios of the PPR with the three-spring model fitted above, the damping ratio for the adhesive material should be known as formulated in Equation (2). Thus, the viscoelastic properties of the adhesive material was measured in this study using Metravib VA2000 Viscoanalyser shown in Figure 10.

The viscoelastic behaviour of the adhesive material can be represented by the complex modulus, E_v^*, as:

$$E_v^* (f,T) = E_v (f,T)(1 + j\eta_v (f,T)) \tag{8}$$

where E_v and η_v respectively represent the elastic modulus and loss factor of the adhesive material (i.e., viscoelastic properties) and $j = (-1)^{0.5}$. It should be noted that both E_v and η_v are the functions of frequency (f) and temperature (T). In order to obtain the viscoelastic properties over a broad range of frequency and temperature, the master curve of the adhesive material was generated by applying the Time-Temperature Superposition principle [9]. the Time-Temperature Superposition allows to obtain the viscoelastic properties for a frequency and temperature different than those measured in the experiment. The viscoelastic properties at any temperature and frequency are computed by:

$$E_v (f,T) = b_T E_v (\alpha_T f, T_{ref}) \tag{9}$$

$$\eta_v (f,T) = b_T \eta_v (\alpha_T f, T_{ref}) \tag{10}$$

where T_{ref} is the reference temperature at which the master curve is produced, and both α_T and b_T are temperature-dependent coefficients. The scaling factor, b_T can be approximated as [10]:

$$b_T = T_{ref} / T \tag{11}$$

whereas the shift parameter, α_T can be described using the original Williams-Landell-Ferry equation:

$$\log_{10}\left(\alpha_T\right) = C_1\left(T - T_{ref}\right)/\left(C_2 + \left(T - T_{ref}\right)\right) \tag{12}$$

where C_1 and C_2 the constants that can be determined by using an optimisation algorithm for the measurements. Note that the Differential Evolution approach [11] was used in this study to determine these constants.
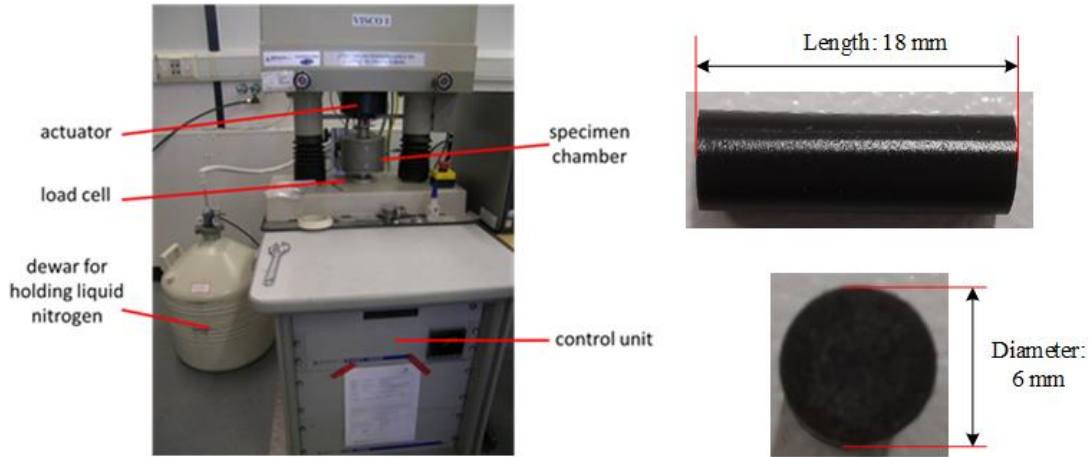

Figure 10: Viscoanalyser used to measure the material properties of the adhesive and sample geometry.

The adhesive material used was Araldite® 2019 epoxy. As can be seen from Figure 10, the cylindrical specimens having 18 mm of length and 6 mm of diameter were considered in the measurements. In the measurements, 6 different specimens were tested for repeatability by applying cycling tension-compression with the amplitude of 0.01% strain. To avoid slipping of specimens, 0.1% of pre-strain was applied to each measurement. Using the dynamic stiffness of each specimen and its geometry, the machine provided the elastic modulus and loss factor reliably over the frequency range 1 to 100 Hz at temperatures between 30° and 190°. Using the measured data, the shift curve was calculated for the adhesive material as shown in Figure 11a.
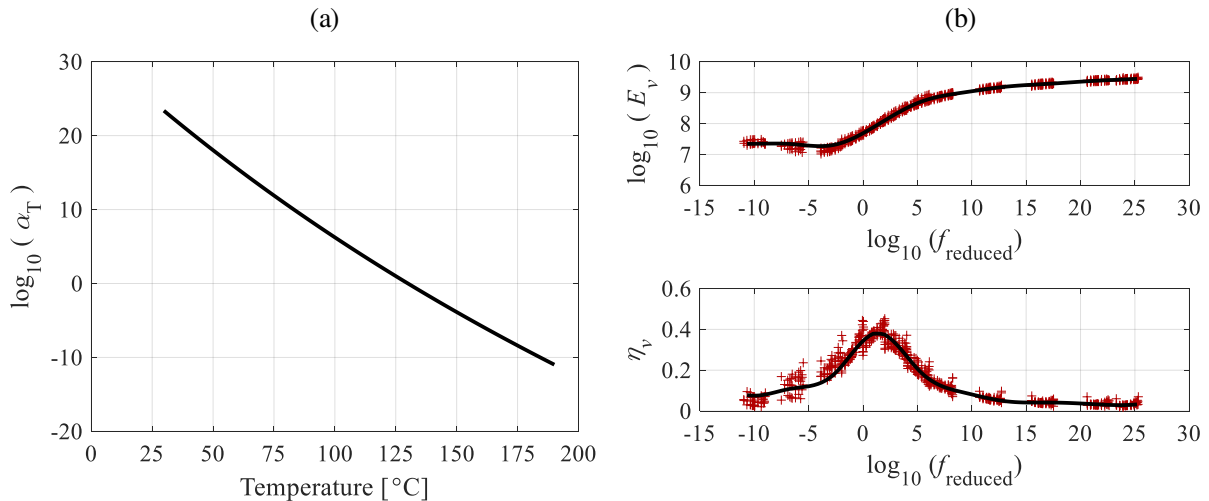

Figure 11: Master curve and measured material properties of the adhesive material.

Using this shift curve and the scaling factor, the master curves were produced for both elastic modulus and damping ratio as shown with black lines in Figure 11b. The measured data (discrete points) is also provided in these plots to show the reliability of the master curves. It should be noted that $f_{reduced} = \alpha_T f$.

4.3   Predicted damping ratios and comparison with experiments

In order to compare the three-spring model fits of the PPR with physical experiments, a modal testing setup was prepared as shown in Figure 12. The modal testing was carried out by placing the PPR in a temperature-controlled environment chamber to measure the damping ratio at different temperatures. The temperature-controlled modal testing aimed to produce noticeable damping ratios by changing the adhesive viscoelastic properties with temperature to achieve U_v/U levels around the peak of U_v/U curve shown in Figure 9. By investigating the adhesive master curve shown in Figure 11, the measurement temperatures were selected as 60, 80, 100 and 110 °C to be around the glass-transition where a higher U_v/U level and thus a higher level of damping ratio can be produced.
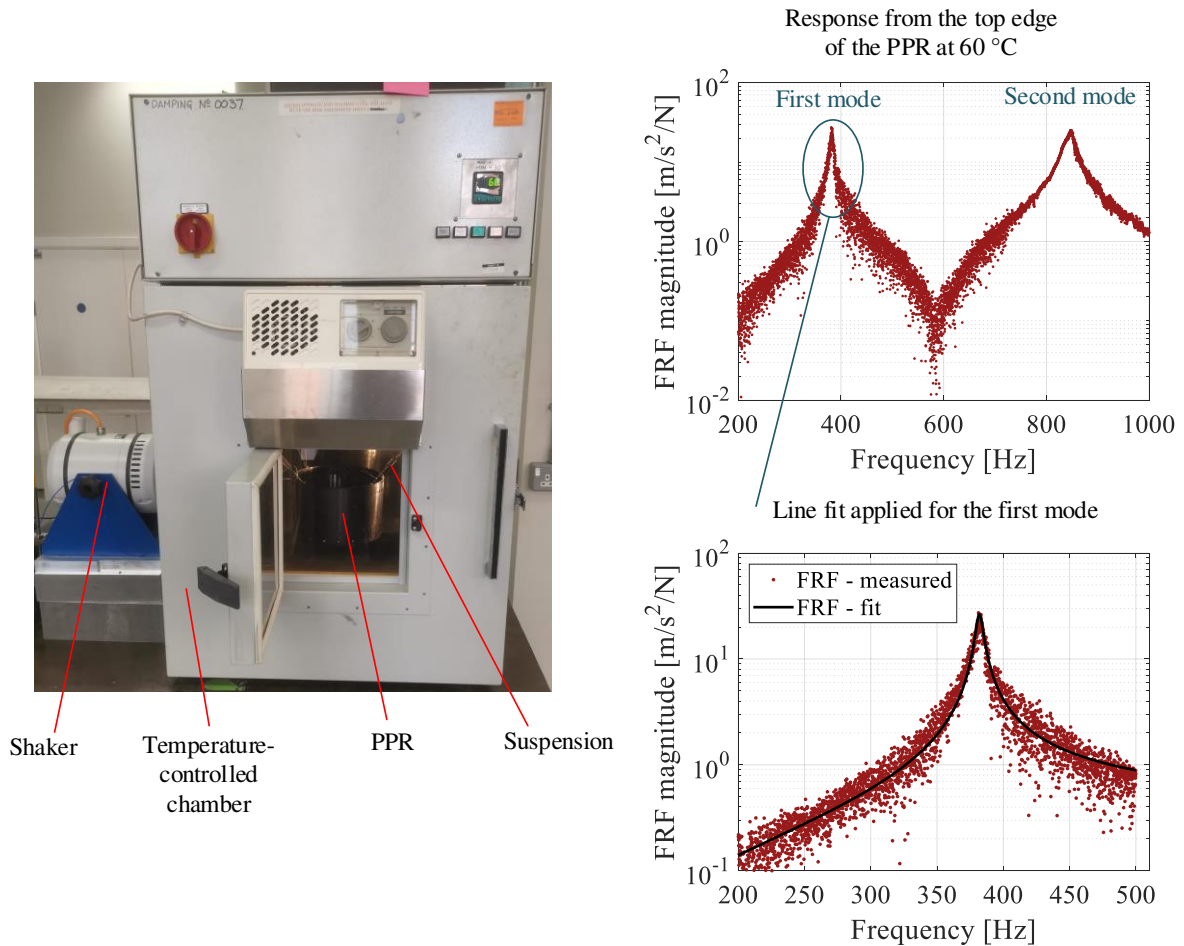

Figure 12: Demonstration of the temperature-controlled modal testing for the PPR.

The PPR was lightly suspended in the temperature-controlled chamber to simulate the free boundary conditions for which the three-spring model fits were achieved for its modes. The PPR was excited at the top edge by a shaker using a sine-sweep excitation, and the forces resulted from this excitation were collected by using a oscilloscope via the force transducer attached between the shaker and the PPR. To obtain point responses, an accelerometer was used at the same position. The time-domain force and acceleration signals were recorded along the excitation duration completed for about 180 seconds with 50 kHz sampling rate. For repeatability, 5 measurements were taken for each temperature case investigated.

For each measurement, the Frequency Response Function (FRF) was evaluated by applying the Discrete Fourier Transform for the collected time-domain signals. A sample average FRF measured at 60 °C can be found in Figure 12 showing the first two casing-dominated modes considered in the three-spring model fits. As can also be seen from Figure 12, to extract the modal damping ratio, the line-fit method [12] which allows obtaining modal properties from a measured FRF was used for the measured complex FRF data around the peak frequencies. The line-fit process was achieved by providing both less than 5% root-mean-square error between the fitted line and the measured FRF data and less than 0.5 Hz error in estimating the peak frequency.

The damping ratios calculated from the measured FRFs involved all dissipative sources within the PPR assembly (such as the joint between the end plate and the casing, the material loss factors of the PPR components). Thus, the damping ratio resulted from only adhesive material should be obtained for sensible comparisons with the three-spring model fits. To quantify the effect of other dissipative sources without involving the effect of the adhesive material, FRF measurements were carried out on the end plate by using simple hammer modal tests. By investigating the first bending mode of the end plate, the modal damping ratio was found to be 0.49%. Assuming that the other dissipative sources other than the adhesive material are not significantly affected by temperature and frequency changes, this damping ratio was subtracted from the measured damping ratios of the casing-dominated modes. The results are summarised in Table 5 as a function of temperature for each mode considered.

To relate k_v in the three-spring model fit with the elastic modulus changes of the adhesive material and thus conduct the appropriate comparisons, the maximum and minimum extremum points observed in Figure 8 and Figure 11 were used by simply scaling the elastic modulus value at the investigated temperature to the corresponding k_v value. These are also provided in Table 5.

Table 5: Comparison of predicted PPR modal damping ratios with physical experiments.

Mode	Properties		T [°C]			
			60	80	100	110
1	From material properties	η_v [%]	4.0	4.6	9.6	13.6
		$(E_v\text{-min}(E_v))/(\max(E_v)\text{-min}(E_v))$ [-]	0.70	0.58	0.37	0.27
	From three-spring model fit	k_v [in terms of k_s]	2.70	1.50	0.46	0.26
		U_v/U [-]	0.09	0.11	0.12	0.09
	Comparison	ζ – predicted [%]	0.18	0.26	0.58	0.61
		ζ – measured [%]	0.21	0.39	0.55	0.74
2	From material properties	η_v [%]	4.0	4.6	9.2	12.8
		$(E_v\text{-min}(E_v))/(\max(E_v)\text{-min}(E_v))$ [-]	0.72	0.59	0.39	0.30
	From three-spring model fit	k_v [in terms of k_s]	3.20	1.30	0.54	0.30
		U_v/U [-]	0.14	0.19	0.20	0.18
	Comparison	ζ – predicted [%]	0.28	0.44	0.92	1.15
		ζ – measured [%]	0.36	0.55	0.85	1.16

The measured damping ratios presented in Table 5 show that the damping ratio of the second mode is consistently higher than the first mode for any temperature as estimated by comparing U_v/U curves in Figure 9. It is clear that the measured damping ratios of both modes increase with temperature as the adhesive material provides more damping when the temperature approaches to the glass-transition (see Figure 11a for justification). The comparison of the predicted damping ratios with those measured indicates that the three-spring model fits successfully represent the modal damping changes with temperature and the predictions are fairly accurate despite many adhesive connections and complicated structure of the PPR. It

can be seen that the measured damping ratios are predicted with a varying level of error. The source of error can be attributed to the listed factors:

i. difference in the estimated mode frequencies of the PPR with the FEM model,
ii. effect of other damping mechanisms in the PPR,
iii. error in the line-fit method used to extract the damping ratio from a measured FRF,
iv. experimental errors while measuring FRFs.

5   Conclusions

This paper shows that the sensitivity of a structure to the stiffness of viscoelastic elements within it can be represented using a three-spring model. Even if the structure has a complex geometry, the three-spring representation gives a good quality fit on a mode-by-mode basis. The fitted three spring model can then easily be used to estimate the damping present in the mode.

The effectiveness of this approach is first shown by comparing results for a beam using the well-known RKU method with those from the three-spring approach. In this study, it is also shown that the effect of a thin viscoelastic layer can be represented in finite element analysis using the host structure and the constraining layer. The viscoelastic layer is not modelled, but instead represented using a scaled value of the contact stiffness – a parameter available in many commercial FEM packages.

The validation of the approach is also demonstrated by investigating the modal properties of a complex composite element in an electric machine containing many thin viscoelastic layers. Using the three-spring approach along with the finite element model using the penalty method, a close agreement between measured and predicted modal damping levels was achieved.

Overall, the ability of the three-spring model to match the sensitivity of the relevant system natural frequency to the stiffness of the viscoelastic material is the basis for the success of the method.

Acknowledgements

References

[1]   D. Ross, E.E. Ungar, E.M. Ungar, Damping of plate structural vibrations by means of viscoelastic laminae, in: Structural Damping, Pergamon Press, New York, 1960.

[2]   A.D. Nashif, D.I.G. Jones, J.P. Henderson, Vibration Damping, First, John Wiley & Sons, New York, 1985.

[3]   Y.S. Jeung, I.Y. Shen, Development of isoparametric, degenerate constrained layer element for plate and shell structures, AIAA Journal 39 (2001) 1997–2005. https://doi.org/10.2514/2.1192.

[4]   M.L. Soni, F.K. Bogner, Finite element vibration analysis of damped structures, AIAA Journal 20 (1982) 700–707. https://doi.org/10.2514/3.51127.

[5]   E.R. Marsh, L.C. Hale, Damping of flexural waves with imbedded viscoelastic materials, J Vib Acoust 120 (1998) 188–193. https://doi.org/10.1115/1.2893803.

[6]   V.R. Buravalla, J.A. Rongong, A.A. Goruppa, G.R. Tomlinson, F.R. Jones, Enhancement and evaluation of damping performance in layered CLD type coatings, in: D.J. Inman (Ed.), Proceedings Volume 4331, Smart Structures and Materials 2001: Damping and Isolation, 2001: pp. 198–208. https://doi.org/10.1117/12.432704.

[7]   P.J. Torvik, B. Runyon, Modifications to the method of modal strain energy for improved estimates of loss factors for damped structures, Shock and Vibration 14 (2007) 339–353. https://doi.org/10.1155/2007/710498.

[8]   Ansys, Academic Research Mechanical, 2022 R2, (2022).

[9]   J.D. Ferry, Viscoelastic Properties of Polymers, Third, John Wiley and Sons, New York, 1980.

[10]   P.E. Rouse, A theory of the linear viscoelastic properties of dilute solutions of coiling polymers, J Chem Phys 21 (1953) 1272–1280. https://doi.org/10.1063/1.1699180.

[11]   R. Storn, K. Price, Differential evolution – a simple and efficient heuristic for global optimization over continuous spaces, Journal of Global Optimization 11 (1997) 341–359. https://doi.org/10.1023/A:1008202821328.

[12]   D.J. Ewins, Modal Testing: Theory, Practice and Application, Second, Research Studies Press Ltd., Hertfordshire, 2000.